Metall. Res. Technol. **119**, 520 (2022)

https://doi.org/10.1051/metal/2022059

&Metallurgical Research Technology

Available online at:
www.metallurgical-research.org

Regular Article

Open Access

Effect of cooling rate on the microstructures of three low carbon alloys with different manganese and molybdenum contents

Anna Benarosch[1,2,*], Bernard Marini[1], Caroline Toffolon-Masclet[1], Zofia Trzaska[2], Estelle Meslin[1], and Ivan Guillot[2]

[1] CEA, Energy Division, Applied Sciences and Simulation for Low Carbon Energy, Department of Materials for Nuclear Applications, 91191 Gif sur Yvette cedex, France
[2] Univ Paris Est, CNRS, ICMPE, UMR 7182, 94320, Thiais, France

Received: 16 April 2022 / Accepted: 9 June 2022

Abstract. Low-alloy 16 to 20MND5 steels are used for the production of nuclear reactor components. During manufacturing, austenitization is followed by a quench; different types of microstructures are formed during this step. Characterizing the impact of Mo and Mn and of cooling rate on these microstructures can help understand how mechanical properties will evolve during tempering and ageing. The impact of molybdenum and manganese, as well as the impact of the cooling rate, were studied on microstructures of three model alloys: FeCMo, FeCMn and FeCMoMn. This was done using continuous cooling transformation (CCT) diagrams and electron backscattering diffraction (EBSD) characterizations. FeCMoMn was found to be a good model for 16 to 20MND5 steels, based on its CCT diagram and hardness. The presence of molybdenum or manganese did not modify the misorientation angle/axis pairs of martensite. In bainitic microstructures however, the presence of Mn seemed to favor the presence of block boundaries with a misorientation about 59° [433]. On the prior austenitic grain (PAG) level, the impact of the cooling rate was rather continuous, from martensite to slowly cooled bainite, and the same regardless of the composition, with the presence of block and sub-block boundaries. The microstructure became coarser with decreasing cooling rate, with fewer crystallographic orientations per PAG.

Keywords: low-alloy steel / continuous cooling transformation / electron backscattered diffraction (EBSD) / phase transformation / misorientation

1 Introduction

Low-alloy steels such as 16 to 20MND5, similar to A508 steels, are commonly used for the production of nuclear pressure vessels, pressurizers and steam generators. 16MND5 contains 0.16wt.% of carbon while 20MND5, 0.20wt.% of C. Molybdenum and manganese are, with nickel, the main alloying elements.

A good knowledge of the impact of the alloying elements and of the cooling rate on the microstructure itself appears to be of importance for two reasons. First, during manufacturing, segregation in carbon and alloying elements is observed in large ingots, at a macroscopic to a microscopic scale, which can locally alter the expected properties [1–3]. Furthermore, while a bainitic microstructure is targeted during the manufacturing of the components, a gradient of microstructures forms during the quench: due to the large thickness, the cooling rate is not homogeneous. Microstructures from allotriomorphic ferrite to martensite can be obtained potentially with very different mechanical properties after tempering at about 650 °C for several hours. Second, during the plant life, the component is subjected to thermomechanical exposure for decades and, for the vessel especially, to neutron irradiation. Due to these service conditions, solute alloy elements and impurities segregate and precipitate. They are the cause of embrittlement mechanisms which can depend, to some extent, on the microstructure [4–8]. Therefore, the heterogeneities in chemical composition and in microstructure can potentially be problematic for estimating the mechanical properties of the whole component after production, and during ageing.

Previous studies attempted to understand the influence of alloying elements on bainite and on martensite in low-alloy steels. For instance, an increasing amount of molybdenum or manganese leads to a finer bainitic microstructure [9–11]. This is explained by the fact that Mo and Mn decrease the bainite transformation temperature [10–12]. Other studies reported that the martensite formation depends on the Mn content [13] and that an increasing amount of Mo or Mn decreases the martensite

* e-mail: anna.benarosch@gmail.com

Table 1. Composition of the high-purity alloys FeCMo, FeCMn and FeCMoMn.

	C (wt%)	Mo (wt%)	Mn (wt%)	P (wt%)	N (wt%)	O (wt%)	S (wt%)
FeCMo	$0.18 \pm 0.02\%$	$1.0 \pm 0.08\%$	–	<0.005%	<0.003%	<0.001%	<0.001%
FeCMn	$0.20 \pm 0.02\%$	–	$1.47 \pm 0.08\%$	<0.004%	<0.003%	<0.001%	<0.001%
FeCMoMn	$0.19 \pm 0.02\%$	$1.14 \pm 0.05\%$	$1.46 \pm 0.05\%$	<0.004%	<0.003%	<0.001%	<0.001%

formation temperature [10,14]. In addition, Mo is known to shift ferrite precipitation towards slower cooling rates [15,16]. A systematic study of the effect of several alloying elements including Mo and Mn demonstrated that neither Mo nor Mn have an impact on the martensitic hardness [17]. Maki et al. [18] investigated the impact of Mo and Mn on lath martensite morphology using model ternary Fe-C-X (X=Mo or Mn) alloys. Solely based on optical observations, they concluded that an addition of about 1wt.% of Mo or Mn does not impact the martensite packet size. When a finer characterization of the bainitic or martensitic microstructures is performed [19–22], the impact of Mo or Mn is not explored.

As for the influence of the cooling rate on microstructural features, little information is available in literature. Su et al. [23] combined dilatometric and electron backscattered diffraction (EBSD) measurements, but only for constituent identification. Graf et al. [24] used EBSD to investigate the influence of the cooling rate on martensite on a low-alloy steel. They found no significant dependence of the cooling rate on the block and packet.

The present work is a contribution to complement the available information in literature. It also aims at improving the current understanding of the role of the Mo and Mn on the microstructure, as a function of the cooling rate in low alloy steels. To isolate the influence of each alloying element, two ternary high-purity model alloys, FeCMo and FeCMn, and one quaternary high-purity model alloy, FeCMoMn were investigated. Continuous cooling transformation (CCT) diagrams were established to study the influence of the cooling rate on the microstructure of these alloys. The obtained microstructures were characterized by EBSD. All the alloys contain a targeted concentration in carbon of 0.2wt.%.

2 Materials and methods

2.1 Production of the high-purity model alloys and characterization of the received material

Each chemical element was first purified: they were melted one after the other using high frequency electromagnetic induction under successive gas fluxes. The first flux was oxygen, then hydrogen and argon. The pure chemical elements were then melted together to produce an ingot, which was homogenized by melting it again two more times. The ingot was shaped with a drop hammer and the final rod-geometry was obtained using a rotary forging machine. A final step of recrystallization was performed at 860 °C for 2 h under a dynamic flux of argon.

The composition of the manufactured alloys was controlled by chemical analysis, see Table 1. Segregation in Mo and Mn existed in the materials upon reception, which formed during the production of the ingot. After austenitizing (see Sect. 2.2), the maximum concentrations measured in Mo and Mn were about 2 wt.%.

2.2 Dilatometry measurements

The samples were directly taken from the as-received rods. They have a cuboid shape, with a size of $7.6 \times 7.6 \times 2\,mm^3$ for FeCMo and $8.8 \times 8.8 \times 2$ mm^3 for the FeCMn and FeCMoMn alloys. The chamber was purged three times with helium before any thermal treatment. Austenitization was divided into two steps: a first step of homogenisation and a second step at an austenitization temperature close to the industrial one. The two steps are described as follows:

- *Homogenisation.* The sample was heated at $1.5\,°C.s^{-1}$ until reaching 1200 °C. The sample was held at this temperature for 5 min.
- *Industrial austenitization temperature.* The sample was cooled at $300\,°C.s^{-1}$ until reaching 890 °C. The sample was held at this temperature for 5 min.

The targeted cooling rates were obtained by flowing helium in the chamber. For cooling rates of $100\,°C.s^{-1}$ or more, helium was first cooled by liquid nitrogen before injection. Transformation temperatures were determined using the deviation from the straight line method. After testing, the dilatometric samples were polished and cut in half to observe their section by light optical microscopy. These sections were polished and etched with 4% nital. The Vickers hardness was measured on at least 15 prints for each sample with a load of 200 gf held for 10 to 15 s.

2.3 Electron backscattered diffraction

The section of the dilatometric samples was polished using a diamond suspension down to 3 µm grade and then polished with a colloidal silica suspension. The EBSD analyses were done with a MEB FEG JEOL JSM and a MEB FEG Zeiss Sigma HD, both equipped with a Bruker e-Flash HR EBSD detector. Several mappings were done for each sample so that the total area analyzed is 2.1 mm^2 with a step of 1µm. The data was acquired with the Bruker Esprit software. To measure the average size of the prior austenite grains (PAG), a reconstruction was carried out using the method developed by Cayron et al. [25] on the software ARPGE 1.2. EBSD data was treated with HKL Channel 5 provided by Oxford Instruments. A Greninger-Troiano orientation relationship was assumed between austenite and ferrite for the reconstruction. The size of the prior austenite grains of the model alloys was reconstructed from EBSD measurements on the martensitic microstructure cooled at $300\,°C.s^{-1}$.

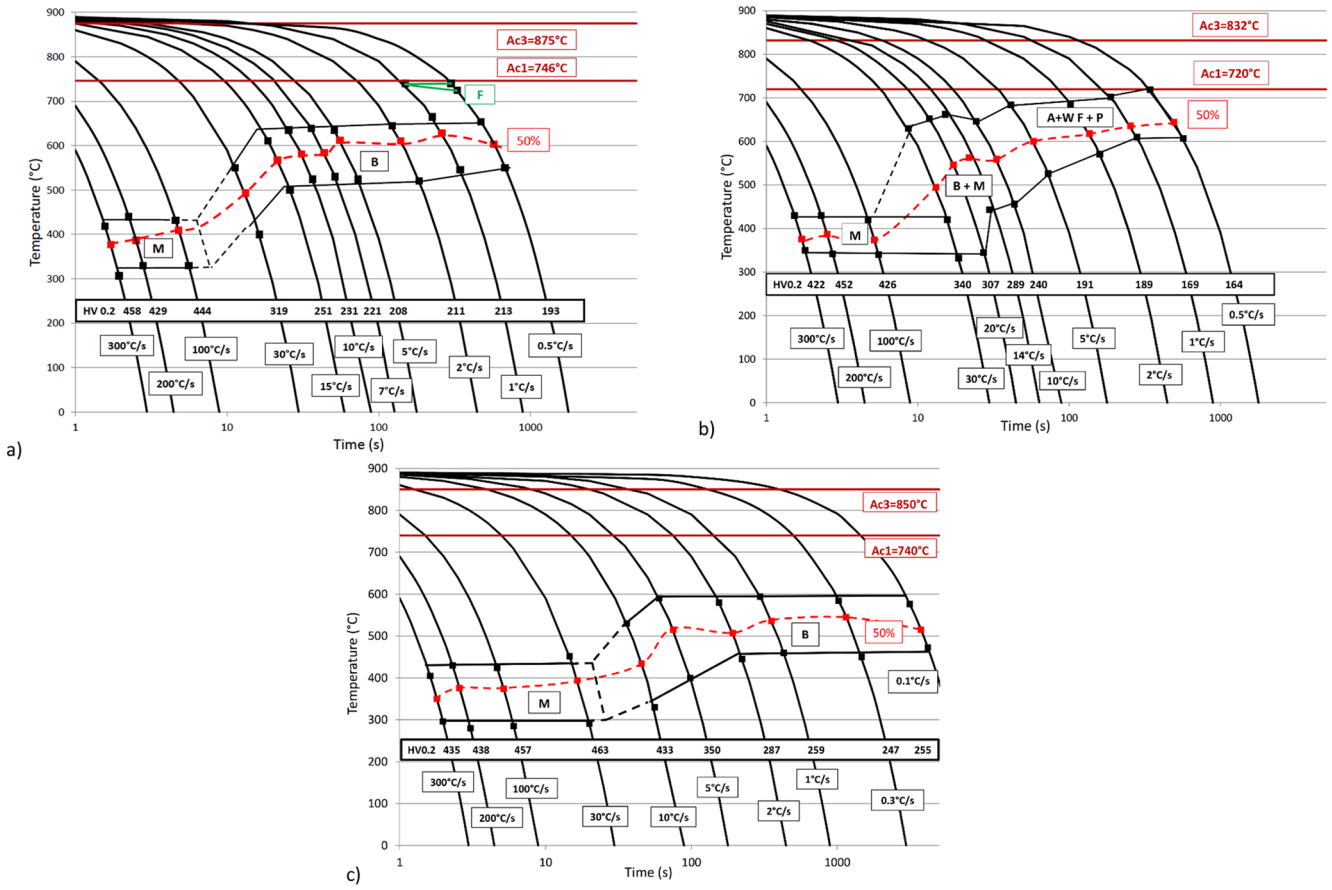

Fig. 1. CCT diagrams for (a) FeCMo, (b) FeCMn and (c) FeCMoMn B=Bainite, M=Martensite, A+W F=allotriomorphic and Widmanstätten ferrite, P=pearlite, F=ferrite.

The misorientation angle distributions are the result of the average of all the mappings. Distributions with a minimum of 5° or 45° are presented: misorientation angles with a value inferior to the minimum were disregarded for the frequency calculation. The misorientation axis distributions in inverse pole figures were solely taken from one of the mappings. However, for a given sample, the misorientation axis distributions in inverse pole figures were the same for every mapping. The misorientation axis distributions indicate the axis along which the misorientation is, in a given angular interval. The axes are displayed in the crystal coordinate system. The densities are expressed relative to that from a random distribution [26], they are calculated in terms of multiple uniform density (mud).

EBSD analysis of the microstructures was used to derive the misorientation between neighboring grains in terms of a pair of angle and rotation axis. These pairs were compared to the expected pairs related to phase transformation models. The microstructures can have with austenite a Kurdjumov-Sachs (KS) [27] orientation relationship (OR), a Nishiyama-Wasserman (NW) [28] OR or a Greninger-Troiano (GT) [29] orientation relationship. Misorientation can be calculated between variants bearing one of these OR. The misorientation angle/axis pairs for KS/KS, NW/NW, KS/NW and GT/GT misorientation relationships are listed in supplementary material, in Table S1.

The prior austenite grains examined in detail in the present work were chosen to have a diameter close to the average size of the prior austenite grains.

3 Results

3.1 Phase transformation and CCT diagrams

The CCT diagrams of the model alloys are presented in Figure 1 and the CCT diagram of a 20MND5 steel is reported by Marini et al. [7]. They cover cooling rates from 300 °C.s^{-1} to 0.5 °C.s^{-1} for ternary alloys, and down to 0.1 °C.s^{-1} for FeCMoMn and the 20MND5 alloy. All three model alloys show a prior austenite grain size with an average between 74 and 92 µm. The average PAG size in the 20MND5 alloy, is about 100µm [7].

FeCMo and and FeCMoMn have somewhat similar CCT diagrams, Figures 1a and 1c. These diagrams are divided into two main domains: one fully bainitic with a rather constant formation temperature, and one fully martensitic. Nevertheless, the transformation temperatures for FeCMo are all higher than those for FeCMoMn in the bainitic domain. For the FeCMn alloy, while there is a fully martensitic domain, there is no fully bainitic domain (Fig. 1b). In this system, for cooling rates between 20 °C.s^{-1} and 10 °C.s^{-1}, the fraction of martensite increases with

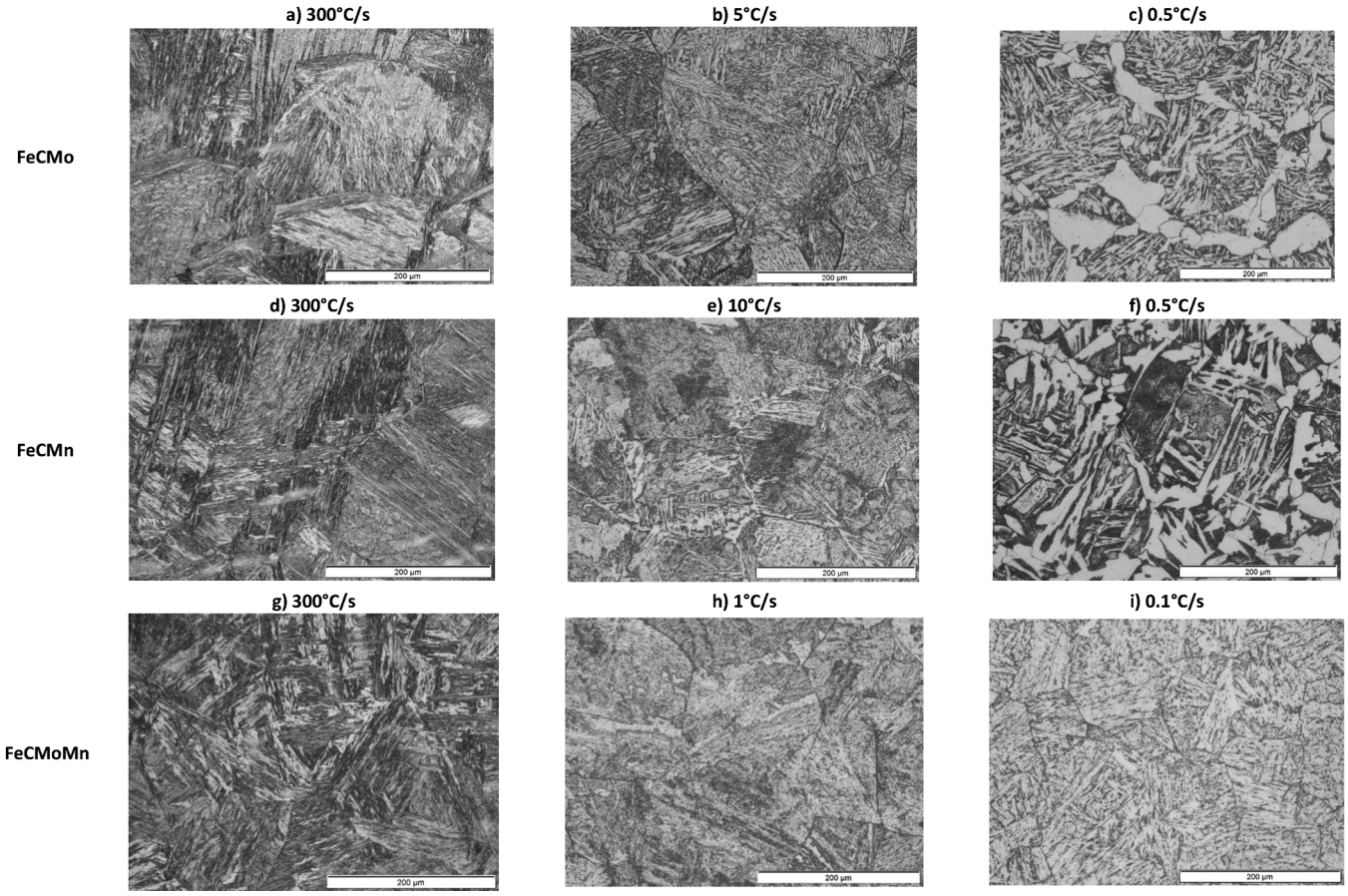

Figure 2. Micrographs for different cooling rate for FeCMo (a,b,c), FeCMn (d,e,f) and FeCMoMn (g,h,i).

cooling rate. At 5 °C.s^{-1}, the FeCMn microstructure is a mix of allotriomorphic and Widmanstätten ferrite (A+WF), with bainite. Below 5 °C.s^{-1}, bainite is replaced by pearlite, see Figure 2f. Observing the presence of allotriomorphic and Widmanstätten ferrite together is not surprising since the Widmantstätten ferritic laths nucleate on allotriomorphic ferrite grains, with a low misorientation angle between them [30,31]. Furthermore, the formation of Widmanstätten ferrite is favored by the large size of the prior austenite grains.

In the fully martensitic domain, the formation temperature (M_s) is close for all the model alloys, with an average value of 430 °C, and the microstructures are similar, see Figures 2a, 2d and 2g. The experimental M_s is comparable to what Andrews empirical equation predicts: 451 °C for FeCMo, 414 °C for FeCMn and 406 °C for FeCMoMn. In that domain, the Vickers hardness is rather constant with close values for all compositions. The presence of Mn increases the martensitic hardenability of the steel, as reported before in literature [16]. Martensitic microstructures can be seen for cooling rates down to 30 °C.s^{-1} or even below in the case of the FeCMn alloy.

Combining molybdenum and manganese decreases the bainite formation temperature (B_s); it is about 650 °C in the ternary alloys, while it is more than 50 °C lower for the FeCMoMn alloy, with an average of 585 °C, see Figure 1a to 1c. Combining both elements also decreases the martensite finish temperature (M_f): in the quaternary alloy, M_f is in average 290 °C, while for the ternary model alloys the average M_f is between 320 °C and 340 °C.

In the FeCMo and FeCMoMn systems, the bainitic microstructure becomes coarser with decreasing cooling rates, according to optical observations, see Figures 2b, 2c and 2h, 2i. In these alloys, bainite is the main constituent even for cooling rates as low as 0.5 °C.s^{-1} for FeCMo and 0.1 °C.s^{-1} for FeCMoMn. Nevertheless, ferrite precipitates at grain boundaries for FeCMo at cooling rates equal to 1 and 0.5 °C.s^{-1} (Fig. 2c).

The FeCMoMn CCT diagram, Figure 1c, and the 20MND5 steel CCT diagram [7] share many similarities. For instance, the martensite and bainite formation temperatures are the same and the cooling rate at which the bainitic domain starts (10 °C.s^{-1}) is also the same. However, the CCT diagram for 20MND5 has a range of cooling rates for which the martensitic and bainitic domains overlap, which is not the case in the quaternary model alloy. Furthermore, ferrite precipitates from 0.3 °C.s^{-1} in the CCT diagram for 20MND5, while no ferrite at grain boundaries is present for FeCMoMn for the lowest cooling rates. This is due to the higher concentration in molybdenum added in the model alloy compared to 20MND5 steel.

Despite small differences, the FeCMoMn and the 20MND5 CCT diagrams are almost the same. It means

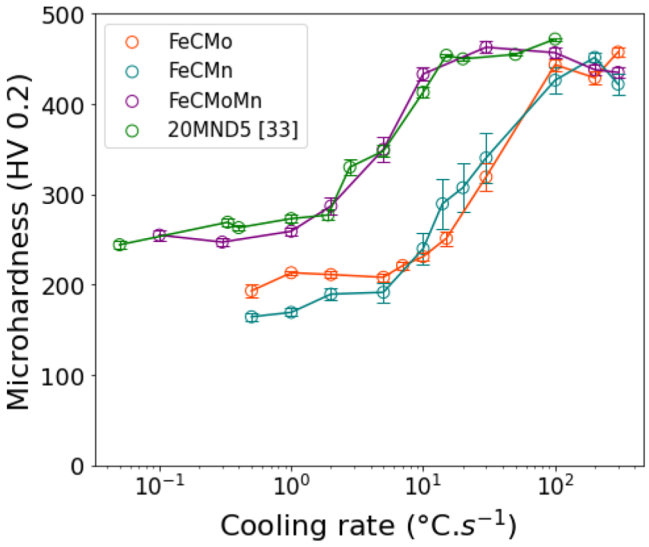

Fig. 3. Microhardness for each composition depending on the cooling rate.

that Mo and Mn play a great role in determining the phase transformations in the 20MND5 alloy, and that the other alloying elements only contribute slightly to determining the diagram.

3.2 Hardness vs cooling rates

The evolution of the Vickers hardness with the cooling rate is displayed in Figure 3. Despite different CCT diagrams, the ternary alloys have similar hardness variations with cooling rate and close hardness values. Adding 1wt.% of Mo or 1.5wt% of Mn has the same effect on hardness for a given cooling rate, despite different microstructures. For example, the FeCMn mix of A+WF and pearlite cooled at 2 °C.s^{-1} has the same hardness as the FeCMo bainite cooled at 2 °C.s^{-1}. For bainitic microstructures and for compositions around 1wt.% of Mo or Mn, Irvine and Pickering have reported that the hardness is expected to be similar [32].

In the quaternary alloy, Vickers hardness variation is the same as for the ternary alloys, but the hardness shifted towards lower cooling rates by a factor of ten. Furthermore, the hardness values for the quaternary alloy are the same as for the 20MND5 steel [33], see Figure 3. Similar CCT diagrams and hardness values indicate that the FeCMoMn alloy can be used as a fair model for studying microstructures of the 16 to 20MND5 steels.

For all three model alloys, the Vickers hardness evolution can be divided into three domains: two domains where hardness is constant and one where hardness increases with increasing cooling rate.

The cooling rates for the first domain are: 5 °C.s^{-1} and less for the ternary alloys, 1 °C.s^{-1} and less for the quaternary alloy. In this domain, the hardness value is constant. The second hardness domain ranges from 10 °C.s^{-1} to a 100 °C.s^{-1} for the ternary alloys, and from 2 °C.s^{-1} until 30 °C.s^{-1} for FeCMoMn. In this domain, the hardness increases with the cooling rate. In the FeCMn alloy, this can be explained by the increasing proportion of martensite until reaching a fully martensitic microstructure at 100 °C.s^{-1}. For FeCMo and FeCMoMn however, the microstructure is fully bainitic. The increase in hardness can be explained by a microstructure becoming finer with increasing cooling rate. The third hardness domain corresponds to the martensitic domain. This domain exists from 100 °C.s^{-1} and above for the ternary alloys and above 30 °C.s^{-1} for the quaternary one. The hardness in the martensitic domain is independent of the cooling rate.

Table 2 gives the average hardness values for different types of microstructures, relying on the CCT diagrams. The average martensitic hardness is the same for all the model alloys, meaning it is independent of the type of alloying element, as already reported in [17]. However, the average bainitic hardness is higher in the quaternary alloy than in the ternary alloys; both alloys have a hardness of 240, despite the presence of martensite in the FeCMn composition. Since the bainitic microstructure has a lower formation temperature in the quaternary alloy, this increase in bainitic hardness is due to a microstructure refinement coming from combining the two alloying elements.

3.3 Misorientation angle distributions

Figure 4 shows the misorientation angle distributions for several cooling rates investigated by EBSD, for the FeCMo alloy. Results for the two other compositions can be found in the supplementary material, in Figures S1(a) to S1(d).

In the FeCMo alloy, the distributions can be divided into two groups, see Figures 4a and 4b. The first group of distributions, containing the cooling rates from 300 °C.s^{-1} to 30 °C.s^{-1}, has a high frequency of boundaries misoriented 59°. The second group, containing the cooling rates below 10 °C.s^{-1}, has boundaries with a misorientation 53° and 59° of equal frequency. Most of the time, this group also presents boundaries misoriented 8°, which is not the case for the second group. This classification is also applicable to the FeCMo CCT diagram. The first group corresponds to the martensitic microstructures, except for the microstructure cooled at 30 °C.s^{-1}. The second group corresponds to the bainitic domain. The microstructure cooled at 30 °C.s^{-1}, although in the bainitic domain, has a similar misorientation angle distribution to martensitic microstructures. It is the only cooling rate for which the bainitic formation temperature is lower than for the other bainitic microstructures. This agrees with the distinction found by Gourgues et al. [19] between microstructures formed at high temperature versus microstructures formed at low temperatures.

For FeCMn however, see supplementary material Figures S1(a) and S1(b), the impact of the cooling rate on misorientation angle distributions is different than for FeCMo. The distributions cannot be regrouped according to their microstructure. These distributions essentially represent a continuum. The more the cooling rate decreases, the fewer boundaries with a misorientation 59° there are, and the more boundaries with a misorientation 53° are present. Furthermore, the higher the cooling rate, the lower is the misorientation frequency of 8°. The microstructure cooled at 0.5 °C.s^{-1} even tends towards a random (McKenzie) distribution [34]. Even though the

Table 2. Average Vickers hardness (HV 0.2) according to microstructure for the model alloys, using the CCT diagrams. *The value given for the FeCMn bainite is the hardness of the microstructure cooled at 10°C.s^{-1}, with the least possible martensite.

	FeCMn	FeCMo	FeCMoMn
Martensite			
Average hardness	433 ± 7	443 ± 4	448 ± 3
Cooling rate interval	100°C.s^{-1} to 300°C.s^{-1}	100°C.s^{-1} to 300°C.s^{-1}	30°C.s^{-1} to 300°C.s^{-1}
Bainite			
Average hardness	240 ± 18*	240 ± 3	305 ± 3
Cooling rate interval	10°C.s^{-1}	2°C.s^{-1} to 30°C.s^{-1}	0.1°C.s^{-1} to 10°C.s^{-1}
Ferrite + Pearlite			
Average hardness	179 ± 4	–	–
Cooling rate interval	0.5°C.s^{-1} to 5°C.s^{-1}	–	–

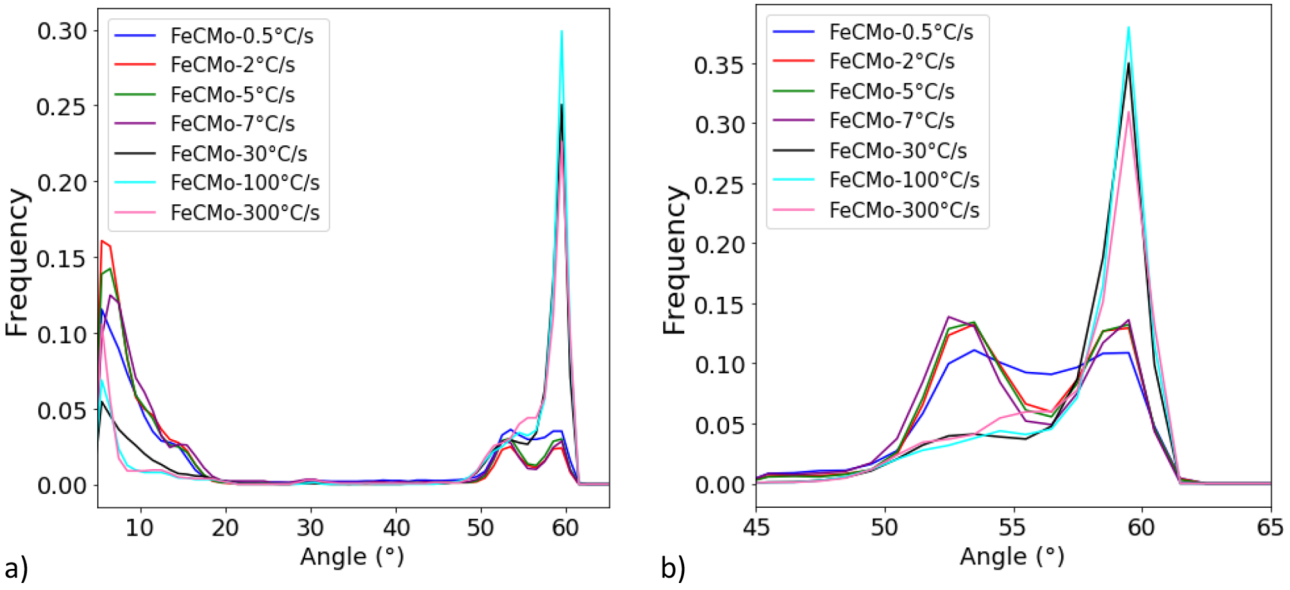

Fig. 4. Misorientation angle distributions for the FeCMo composition with a minimum at 5° (a) and a minimum at 45° (b). Misorientation angles with a value inferior to the minimum are disregarded for the frequency calculation.

Widmanstätten ferrite is known to have a Kurdjumov-Sachs (KS) relationship with the austenite phase [35], the large amount of pearlite and allotriomorphic ferrite in the sample, see Figure 2f, explains why the distribution tends toward a McKenzie distribution [26].

Although FeCMoMn and FeCMo have similar CCT diagrams, the evolutions of the misorientation angle distributions with cooling rate differ, see supplementary material figures S1(c) and S1(d). For microstructures from 300 °C.s^{-1} to 2 °C.s^{-1}, the frequency of boundaries misoriented 59° increases with decreasing cooling rate, while for FeCMo and FeCMn it is the opposite. This is due to a higher proportion of boundaries with a low misorientation and of boundaries with a misorientation between 50° and 57° for the highest cooling rates. Nevertheless, the distributions of microstructures obtained for a cooling rate lower than 2 °C.s^{-1} tend to have similarities to the FeCMo bainitic distributions: the most frequent misorientation for boundaries are 53°, 59° or 8°. Therefore, the FeCMoMn bainitic microstructures could be sorted into a group with microstructures from 10 °C.s^{-1} to 2 °C.s^{-1} and another one with microstructures cooled from 1 °C.s^{-1} to 0.1 °C.s^{-1}. However, this classification could not be explained by what is reported in the CCT diagram, since all these microstructures have about the same formation temperatures. The peak observed at 30° is due to an error in indexation of the Kikuchi patterns [19].

The evolution of the misorientation angle distributions with cooling rate differs for each composition, even for FeCMo and FeCMoMn alloys which have somewhat similar CCT diagrams.

4 Discussion

4.1 The martensitic domain

The martensitic microstructures cooled at 300 °C.s^{-1} of each model alloy are compared. Figures 5a and 5b show

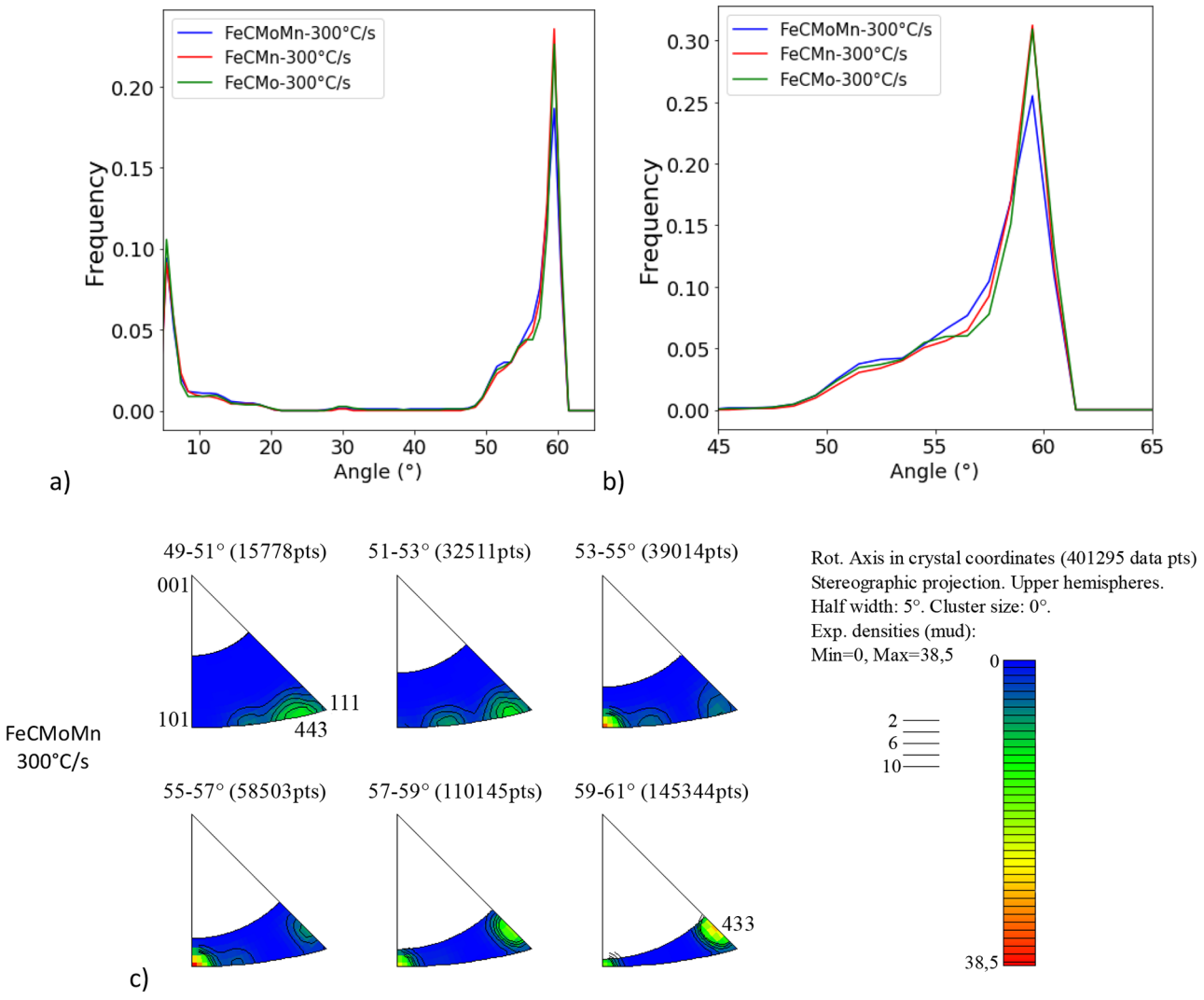

Fig. 5. EBSD on the martensitic domain: misorientation angle distribution with a minimum of 5° (a) and a minimum of 45° (b). Misorientation angles with a value inferior to the minimum are disregarded for the frequency calculation. (c) is the misorientation axis distribution for the FeCMoMn composition cooled at 300 °C.s^{-1}.

Table 3. High angle/axis misorientation pairs measured for the martensite of the three model alloys compared to the closest misorientation pairs from GT/GT and KS/NW MR. The pair marked with (*) is less present than the others. The angle value given in parenthesis is the deviation from the specified axis.

Martensite	Model Alloys			GT/GT		KS/NW	
Angle	51° ± 2*	55° ± 2	59° ± 2	54.3°	60.2°	54.7°	60.2°
Axis (Offset angle)	443*	101	433	101 (0°)	433 (3.25°)	101 (3.08°)	433 (2.80°)

that all three alloys have similar misorientation angle distributions. Figure 5c displays the misorientation axis distribution in inverse pole figures for the quaternary alloy, for angles superior to 49°; see supplementary material Figures S2(a) and S2(b) for the misorientation axis distributions of the ternary alloys.

All three compositions have similar misorientation axis/angle pairs. The main misorientation pairs are 53−57° [101] and 59°−61° [433]. This is in compliance with the misorientation angle distributions, Figure 5b. These two angle/axis pairs are found for a GT/GT misorientation relationship (MR) [29], see Table 3, and for a KS/NW MR [27,28]. However, they do not exist in KS/KS or NW/NW, see Table S1 in supplementary material [19].

A study in a prior austenite grain (PAG) was performed for each of the three alloys. The conclusions are the same for all three compositions. Figures 6 to 6d is the result of the investigations done in a FeCMoMn PAG selected from the EBSD map, Figure 6a. Three

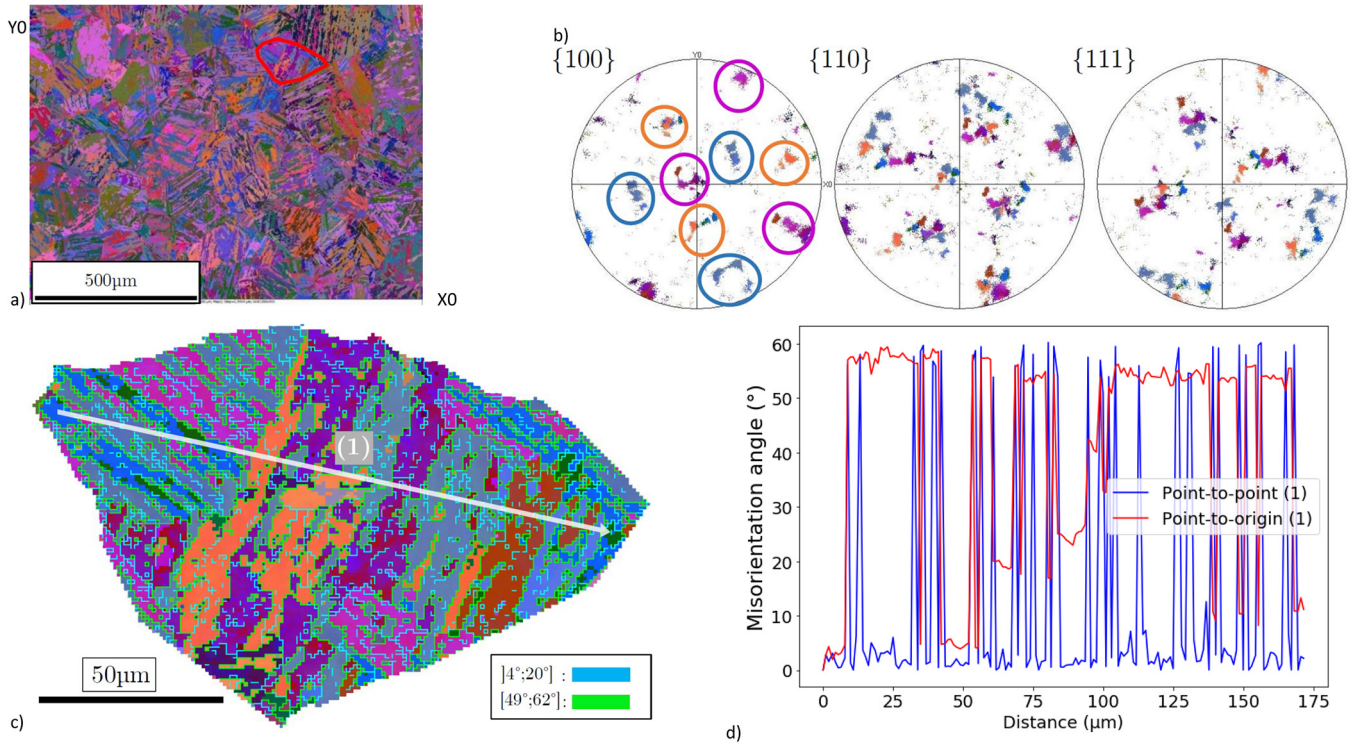

Fig. 6. Study in a prior austenite grain for FeCMoMn 300 °C/s: (a) EBSD map with a prior austenite grain (PAG) in red, (b) {100}, {110} and {111} pole figures of the PAG (stereographic projection), (c) map of the misorientation angles in the PAG with a profile in white, d) misorientation profile in PAG. *(color necessary for print).*

texture components could be identified on the pole figure, Figure 6b, and each of these texture components present between them a misorientation superior to 49°, as illustrated in Figure 6c. Figure 6d shows the misorientation profile associated with the white arrow on Figure 6c. Two types of boundaries can be identified: boundaries misoriented more than 50° and boundaries misoriented about 10°. According to Morito's definition [36], the first type of boundaries is block boundaries, while the low angle boundaries are sub-block boundaries. Inside the blocks and sub-blocks, the misorientation is quite low, lower than 4°, Figure 6c. In the martensitic microstructure, according to Figures 6d and 5b, the most probable block boundary misorientation is 59°.

All three compositions show the same martensitic crystallographic features, as well as similar micrographs and similar hardness values, meaning that neither Mo nor Mn has an impact on the martensitic microstructure.

4.2 The bainitic domain

To study the effect of Mo and Mn on the bainitic domain, the microstructures cooled at 5 °C.s^{-1} for the FeCMo alloy and cooled at 1 °C.s^{-1} for the FeCMoMn composition are compared. They correspond to cooling rates where the bainite transformation temperature is independent of the cooling rate. For the FeCMn alloy, the microstructure with the least martensite and without allotriomorphic and Widmanstätten ferrite is selected; the microstructure cooled at 10 °C.s^{-1} is the closest to a fully bainitic microstructure.

In that domain, the misorientation angle distributions presented in Figures 7a and 7b differ from one composition to another. The Mn-containing alloys have similar distributions with a higher proportion of boundaries misoriented 59°, than what can be found in the FeCMo bainite. In the FeCMo microstructure cooled at 5 °C.s^{-1}, there are as many boundaries misoriented 53° as there are boundaries misoriented 59°. Furthermore, there is a higher tendency to form boundaries misoriented less than 10° in the FeCMo composition. The FeCMo, FeCMn and FeCMoMn misorientation axis distribution for high angles is presented in Figures 7c, 7d and 7e respectively.

When analyzing the misorientation angle/axis pairs, the same differences as for the misorientation angle distributions can be noted. The FeCMo microstructure has two main misorientation angle/axis pairs: 49−53° around the axis [221] and 59−61° [111], which is a Σ3 boundary. These pairs can come from a KS/KS misorientation relationship, see Table 4a, but not from a KS/NW, a NW/NW or a GT/GT MR [19,28], (Table S1 in supplementary material). For the FeCMn alloy, despite being mainly bainitic, similar features to martensite exist with the same misorientation pair 59−61° [433]. As previously stated, this angle/axis pair can come from a KS/NW or GT/GT misorientation relationship, but not from a KS/KS nor NW/NW misorientation relationship [19]. This means that the orientation relationship of the bainitic microstructure with parent austenite may be changing depending on the addition of Mo or Mn. Furthermore, since the 59−61° [433] pair is also present in the FeCMoMn bainitic microstructure, but absent from

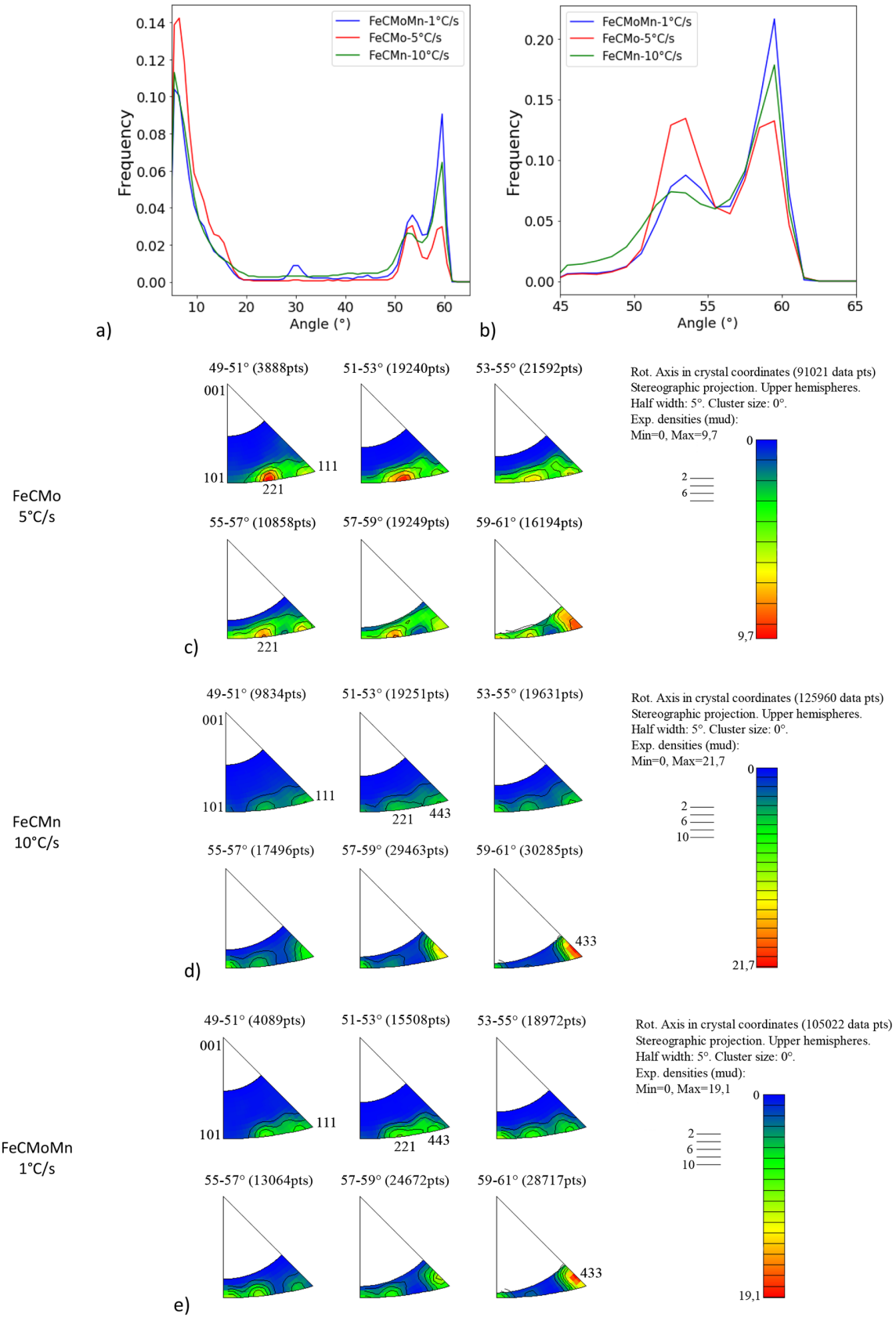

Fig. 7. EBSD on the bainitic domain: misorientation angle distribution with a minimum of 5° (a) and a minimum of 45° (b). Misorientation angles with a value inferior to the minimum are disregarded for the frequency calculation. (c), (d) and (e) are the corresponding misorientation axis distribution.

Table 4.(a) High angle/axis misorientation pairs measured for the bainite of the FeCMo alloy compared to the closest misorientation pairs from KS orientation relationship (OR), and b) high angle/axis misorientation pairs measured for the FeCMo alloy compared to the closest misorientation pairs from KS OR. The pairs marked with (*) are less present than the others.

(a)

Bainite	FeCMo			KS/KS		
Angle	51° ± 2	55° ± 2	59° ± 2	49.5°	51.7°	60°
Axis (Offset angle)	221	221	111	111 (0°)	221 (1.80°)	111 (0°)

(b)

Bainite	FeCMn and FeCMoMn			GT/GT			
Angle	51° ± 2*	55° ± 2*	59° ± 2	50.8°	54.3°	60°	60.2°
Axis (Offset angle)	221* and 443*	101*	433	332 (0.94°)	101 (0°)	101 (0°)	433 (3.25°)

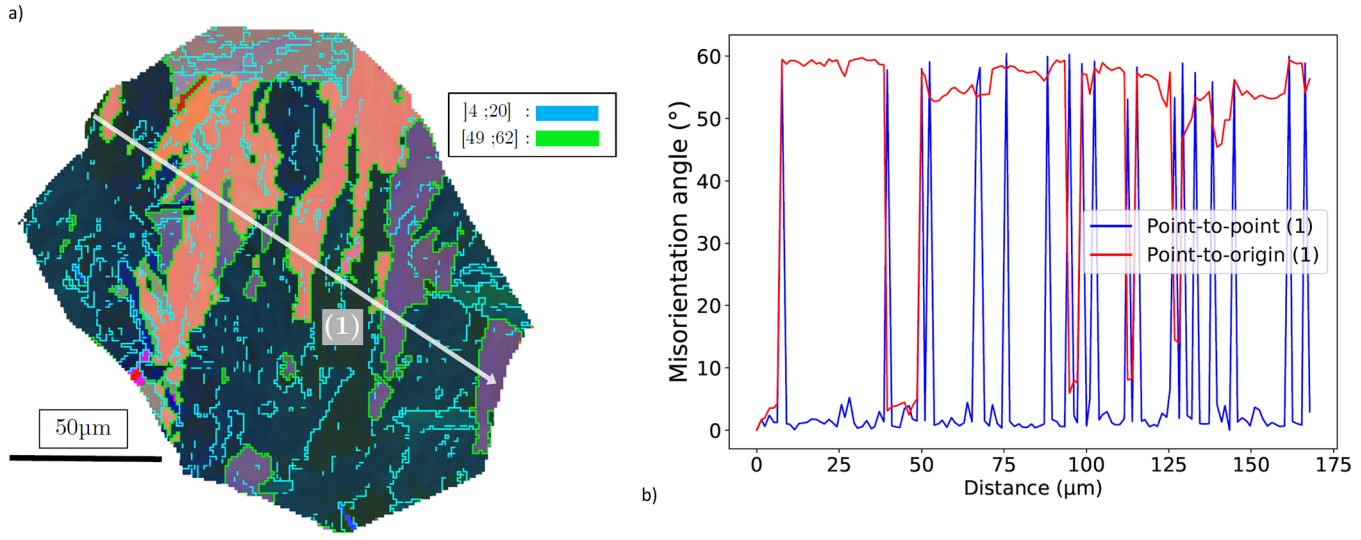

Fig. 8. Study in a prior austenite grain for FeCMoMn 1°C.s^{-1}: a) EBSD map of the misorientation angles in the PAG with a profile in white, and the misorientation profile in PAG (b).

the FeCMo bainitic one, it suggests that the presence of manganese in the bainitic microstructure favors this specific angle/axis pair. The FeCMn and FeCMoMn microstructures share many common misorientation angle/axis pairs that can be found in GT/GT MR, see Table 4b. The pair 49−53° [443] in FeCMn and FeCMoMn can be considered close to the GT/GT pair 50.8° [332] because the [443] axis is close to [332].

Figures 8a and 8b show the misorientation of boundaries in a PAG taken from the FeCMoMn bainitic microstructure. More details can be found in supplementary material, figure S3. A similar investigation was performed in bainitic PAGs in FeCMn and FeCMo and gave similar results.

On the PAG level, the bainitic microstructure has many crystallographic features in common with martensite, despite different misorientation angle and axis distributions. The microstructure is also organized in blocks, separated by boundaries with a misorientation 50° or more, and sub-blocks, with a misorientation from 10° to 20°, see Figures 8a and 8b. Since the FeCMo alloy has a higher frequency of misorientation below 20° than the Mn-bearing alloys, Figure 7a, it means that sub-block boundaries are more frequent in the FeCMo alloy than block boundaries. This can have an impact on the resulting mechanical properties since high angle boundaries can arrest or deviate cracks during cleavage fracture [19,37] while low angle boundaries only show a low angle change in the fissure propagation path inducing a lower dissipation of energy during fracture [38]. The pole figure shows the presence of three texture components with a misorientation 49° at least between each other, see supplementary figure S3(b), as observed for martensite.

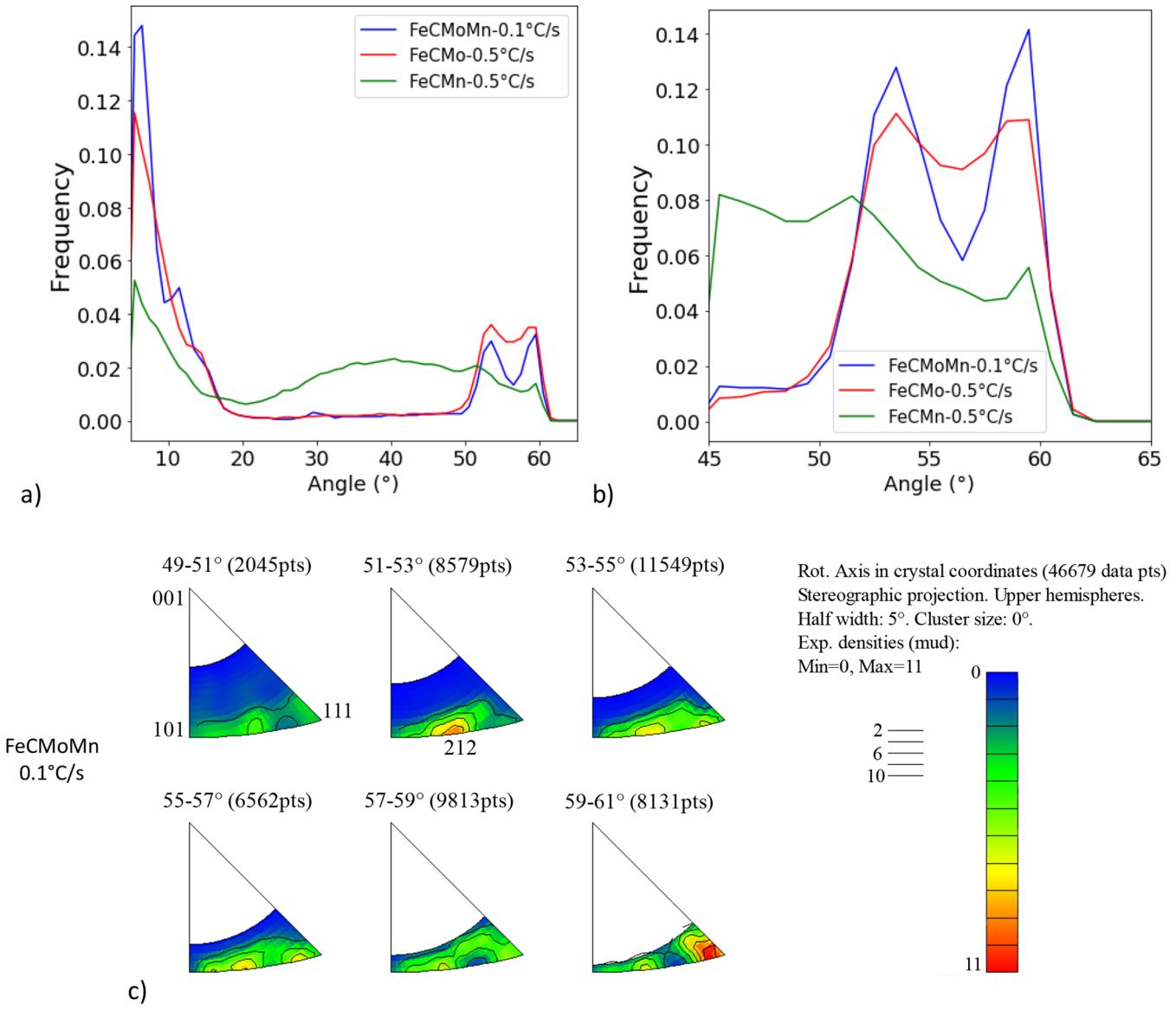

Fig. 9. EBSD on the slowest cooling speeds: misorientation angle distribution with a minimum at 5° (a) and a minimum at 45° (b). Misorientation angles with a value inferior to the minimum are disregarded for the frequency calculation. (c) is the misorientation axis distribution for FeCMoMn composition cooled at 0.1 °C/s (c).

In the bainitic domain, the alloying elements have an impact on the bainitic microstructure despite common crystallographic features at the PAG level.

4.3 Lowest cooling rates domain

In this domain, the microstructures cooled at 0.5 °C.s^{-1} for FeCMo and FeCMn, and the one cooled at 0.1 °C.s^{-1} for FeCMoMn are selected for comparison. The molybdenum-containing alloys have misorientation angle distributions comparable and close to what is observed for the FeCMo cooled at 5 °C.s^{-1}, see Figures 7a-7b and Figures 9a-9b. For FeCMn, the presence of a great proportion of allotriomorphic ferrite and pearlite induces a larger proportion of boundaries with a misorientation between 20° and 49°. Furthermore, boundaries misoriented 59−61° around [433] have disappeared in the FeCMn microstructure, see supplementary Figure S4(b), as well as in the FeCMoMn bainitic microstructure cooled at 0.1 °C.s^{-1}, see Figure 9c . Instead, it has been replaced by Σ3 boundaries. In the case of FeCMn, the presence of Σ3 boundaries can come from a KS/KS MR, since Widmanstätten ferrite has a KS OR.

Despite different microstructures, FeCMn and FeCMoMn share this common twin boundary. Mo seems to have little impact on the selection of the misorientation angle/axis pairs in the FeCMoMn alloy, compared to Mn. In the FeCMo microstructure, the boundaries present at 5 °C.s^{-1}, with a misorientation 49−53° around [221] and Σ3 boundaries, tend to disappear to the benefit of boundaries

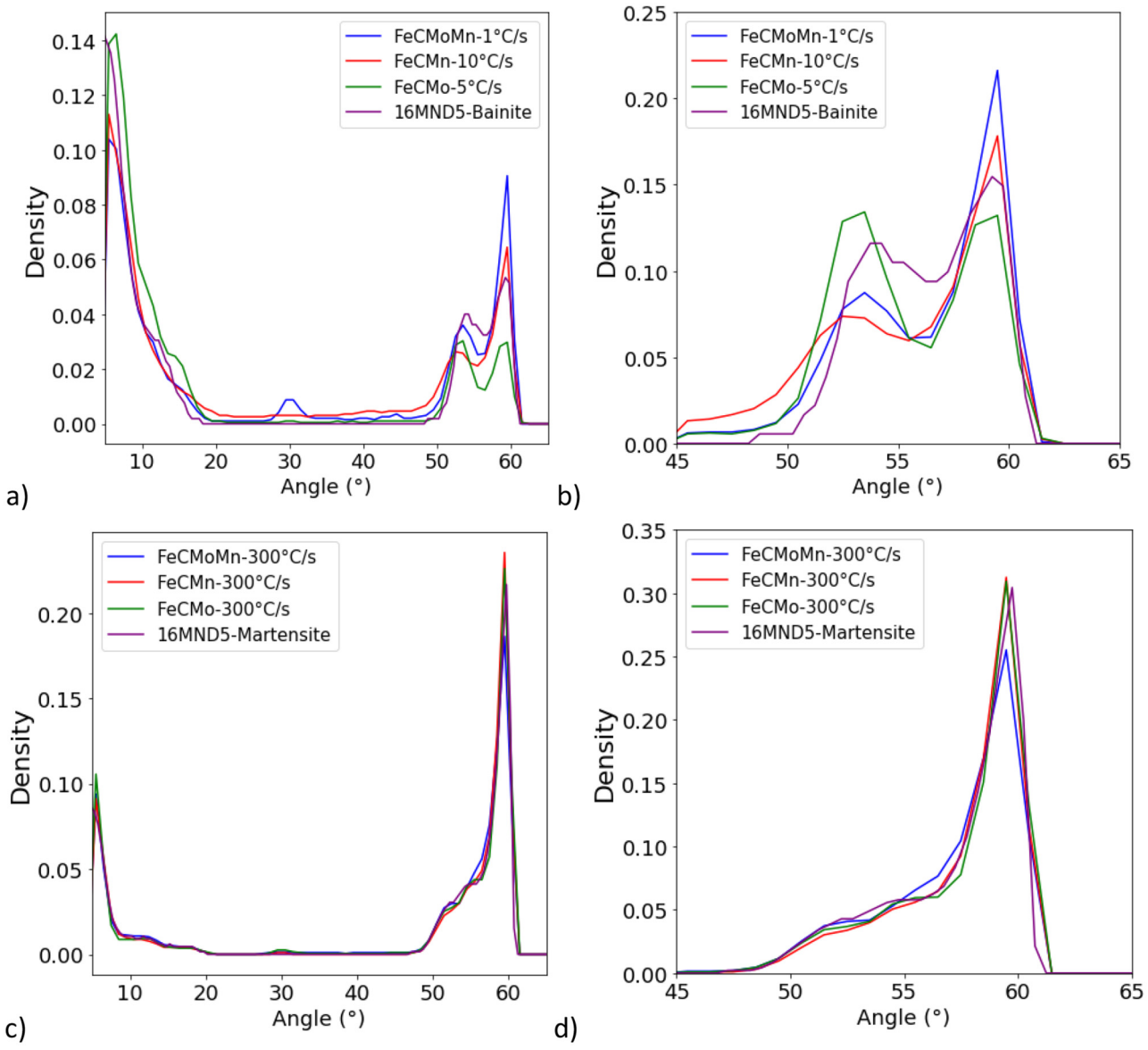

Fig. 10. Comparison with 16MND5 steel: misorientation angle densities with a minimum at 25° and 45° for bainitic microstructures (a and b) and for martensitic microstructures (c and d). Misorientation angles with a value inferior to the minimum are disregarded for the frequency calculation.

with a misorientation 53−57° around [331], which can from a KS/NW and a GT/GT MR [19], see Figure S4a and Table S1 in supplementary material.

Investigation in a FeCMoMn PAG and in a FeCMo bainitic PAG gave similar results. The result for the FeCMoMn PAG can be found in supplementary material Figures S5a to S5d. Due to the microstructure, bainitic misorientation could not be studied in a FeCMn PAG.

The bainitic microstructures in FeCMo and FeCMoMn have three texture components, see supplementary Figure S5b, but some PAG were found with only one or two texture components. As the cooling rate decreases, a narrower range of variants is present per PAG. The supplementary Figure S5d shows that, as for the martensite and the bainite cooled at 1 °C.s^{-1}, block boundaries have a misorientation superior to 50° while sub-blocks a misorientation 10° or less. In that sense, even if the misorientation angle/axis pairs change from a cooling rate to another, it appears that, on the PAG level, the microstructure continuously evolves from martensite to slowly cooled bainite, conserving many crystallographic similarities. At this level, the impact of the cooling rate is continuous and the same regardless of the composition.

As can be shown by comparing supplementary Figure S5c with Figure 8a and 6c, the microstructure becomes coarser with decreasing cooling rate, with fewer high angle boundaries, meaning blocks are getting larger. In these large blocks, the density of sub-blocks boundaries is not increased with decreasing cooling rate, as shown in Figure 8a and supplementary Figure S5c.

4.4 Model and 16MND5 alloys

The misorientation angle densities of 16MND5 bainite and martensite are compared with the model alloys densities, in Figure 10. Density means the frequency is divided by the bin size. It is necessary in this case to compare the frequency distributions because the bin values are different for the 16MND5 and the model alloys distributions. The misorientation angle distributions of the model alloy and of 16MND5 bainite, see Figures 10a and 10b, are similar. The 16MND5 bainite, see Figure 10a, presents a high proportion of low angle boundaries misoriented 8°, as the FeCMo bainite. Regarding the high angle boundaries, that is to say block boundaries, there is a nearly equal proportion of boundaries misoriented 53° and 59°, Figure 10b. The 16MND5 bainite presents a higher proportion of boundaries misoriented 53° than for the Mn-bearing model alloys.

As for the martensitic microstructures, the distributions of the 20MND5 steel and of the model alloys are quite similar, see Figures 10c and 10d. Boundaries misoriented 60° are the most frequent in the 16MND5 martensite, as in the model alloys. The boundaries misoriented 53°, 55° and 60° are present in similar proportion in the 16MND5 martensite as in the model alloys (Fig. 10d).

Taking into consideration the misorientation angle distributions for both bainite and martensite, the investigated ternary and quaternary alloys are good models for the 16 to 20MND5 steels.

5 Conclusions

The microstructures of three model alloys were studied: two ternary FeCMo and FeCMn and one quaternary FeCMoMn. The influence of the cooling rate and of the alloying elements were investigated thanks to CCT diagrams and EBSD. This led to the following conclusions:

- The presence of Mo and Mn greatly explains the phase transformations observed in the 16 to 20MND5 alloys, since the FeCMoMn and the 20MND5 CCT diagrams are almost the same. Furthermore, the model quaternary and 20MND5 alloys have similar hardness. FeCMoMn can be considered as a fair model for 16 to 20MND5 steels. This is confirmed by comparing the alloys misorientation angle distributions.
- The average bainitic hardness is higher when combining Mo and Mn. The martensitic hardness is independent of the cooling rate and of the type of alloying element.
- While the FeCMo microstructures can be sorted out between martensitic and bainitic ones based on their misorientation angle distributions, the FeCMn microstructures shows a rather continuous evolution. Finally, for the FeCMoMn alloy, the evolution of the frequency of boundaries with a misorientation 59° increases with decreasing cooling rate, from 300 °C.s^{-1} to 2 °C.s^{-1}. It is the opposite for the ternary alloys. This means the evolution of the misorientation angle distributions with cooling rate differs for each composition.
- In the martensitic microstructures, no effect of Mo or Mn is detected on misorientation angle nor misorientation axis distributions.
- In the bainitic microstructures however, the presence of Mn seems to favor the presence of block boundaries with a misorientation angle/axis pair 59° [433].
- On the PAG level, the impact of the cooling rate is rather continuous and the same regardless of the composition. The microstructure becomes coarser with decreasing cooling rate, with fewer crystallographic orientations in one PAG: three texture components are present for the highest cooling rate, while only one or two texture components per PAG can be found for the slowest cooling rate.

Data availability

The raw and processed data required to reproduce these findings cannot be shared at this time due to legal or ethical reasons.

Acknowledgements. The authors would like to acknowledge the Commissariat à l'Énergie Atomique et aux Énergies Alternatives (CEA) for funding. They wish to thank Jean-Baptiste Delattre from the Commissariat à l'Énergie Atomique et aux Énergies Alternatives (CEA) for providing microhardness data on 20MND5. Thanks are also due to Françoise Barcelo, Amélie Gangloff and Élodie Rouesne from CEA for their help with EBSD measurements. The authors would like to acknowledge Thomas Gilbert for his help with dilatometry, as well as Remy Pires and Julie Bourgon from the ICMPE for their precious help and advice. The authors would like to thank Anna Fraczkiewicz and her team from the Georges Friedel Laboratory of the Mines Saint-Étienne (UMR 5307) for the production of the model alloys. The authors express their gratitude to Yoel Benarosch for his help with English.

Supplementary Material

Table S1: Theoretical angle/axis pairs for KS/KS, NW/NW, KS/NW [39] and GT/GT misorientation relationships. Some rotation axes having irrational indexes, they were approximated by low index crystallographic axes. The offset angle between the actual axes and the low-index axes is specified.

Figure S1: (a) and (c) misorientation angle distributions for FeCMn and FeCMoMn compositions with a minimum at 5° and a minimum at 45° (b and d). Misorientation angles with a value inferior to the minimum are disregarded for the frequency calculation. (*color necessary for print*).

Figure S2: EBSD on the martensitic domain: misorientation axis distributions for the FeCMo composition (a) and FeCMn composition (b). (*color necessary for print*).

Figure S3: Study in a prior austenite grain for FeCMoMn 1°C/s: (a) EBSD map with a prior austenite grain (PAG) in red, (b) {100}, {110} and {111} pole figures of the PAG (stereographic projection), (c) map of the misorientation angles in the PAG with a profile in white, (d) misorientation profile in PAG. (*color necessary for print*).

Figure S4: EBSD for the slowest cooling speeds: misorientation axis distribution for the FeCMo composition (a) and FeCMn composition (b). (*color necessary for print*).

Figure S5: Study in a prior austenite grain for FeCMoMn 0.1°C/s: (a) EBSD map with a prior austenite grain (PAG) in red, (b) {100}, {110} and {111} pole figures of the PAG (stereographic

projection), (c) map of the misorientation angles in the PAG with a profile in white, (d) misorientation profile in PAG. (*color necessary for print*).

The Supplementary Material is available at https://www.metal.org/10.1051/metal/2022059/olm.

References

1. S. Saillet, N. Rupa, C. Benhamou, Impact of large forging macrosegregations on the reactor pressure vessel surveillance program, Fontevraud **6**, 1–13 (2006)
2. E.J. Pickering, H.K.D.H. Bhadeshia, The consequences of macroscopic segregation on the transformation behavior of a pressure-vessel steel, J. Pres. Vessel Technol. Trans. ASME, **136**, 1–7 (2014)
3. F. Barcelo, B. Marini, S. Saillet, et al., Metallurgical characterization of micro-heterogeneities in a 16MND5 forging, Fontevraud **9**, 1–10 (2018). https://www.researchgate.net/publication/328838041
4. L. Zhang, B. Radiguet, P. Todeschini, et al., Investigation of solute segregation behavior using a correlative EBSD/TKD/APT methodology in a 16MND5 weld, J. Nucl. Mater. **523**, 434–443 (2019)
5. J. M. Capus, Temper embrittlement in steel, ASTM STP, **407**, 3–19 (1968).
6. S. Raoul, B. Marini, A. Pineau, Effect of microstructure on the susceptibility of a 533 steel to temper embrittlement, J. Nucl. Mater. **257**, 199–205 (1998)
7. B. Marini, X. Averty, P. Wident, et al., Effect of the bainitic and martensitic microstructures on the hardening and embrittlement under neutron irradiation of a reactor pressure vessel steel, J. Nucl. Mater. **465**, 20–27 (2015)
8. M. Vacek, Effect of various metallurgical microstructures on the response of the nickel-molybdenum-chromium BH 70 steel to neutron irradiation at 285 °C, ASTM STP **909**, 260–278 (1986)
9. H. Hu, G. Xu, M. Zhou et al., Effect of mo content on microstructure and property of low-carbon bainitic steels, Metals **6** (2016)
10. J. Kong, C. Xie, Effect of molybdenum on continuous cooling bainite transformation of low-carbon microalloyed steel, Mater. Des. **27**, 1169–1173 (2006)
11. C. Zhang et al., Effect of Mn content on microstructure and properties of wear-resistant bainitic steel, Mater. Res. Exp. **6** (2019)
12. J.M. Reichert, M. Militzer, Quantifying the effect of Nb and Mo on transformation products using advanced EBSD analysis, HSLA Steels 2015, Microalloying 2015 & Offshore Engineering, 2015, pp. 1–8
13. M.J. Roberts, Effect of transformation substructure on the strength and toughness of Fe-Mn alloys, Metall. Trans. **1**, 3287–3294 (1970)
14. D.-H. Huang, G. Thomas, Structure and mechanical properties of tempered martensite and lower Bainite in Fe-Ni-Mn-C steels, Metall. Trans. **2**, 1587–1598 (1971)
15. S. Khare, K. Lee, H.K.D.H. Bhadeshia, Relative effects of Mo and B on ferrite and bainite kinetics in strong steels, Int. J. Mater. Res. **11**, 1513–1520 (2009)
16. F.B. Pickering, Physical metallurgy and the design of steels. Applied Science Publishers Ltd., 1978
17. R.A. Grange, Estimating the hardenability of carbon steels, Metall. Trans. **4**, 2231–2244 (1973)
18. T. Maki, K. Tsuzaki, I. Tamura, The morphology of microstructure composed of lath martensites in steels, Trans. ISIJ **20**, 207–214 (1980)
19. A.F. Gourgues, H.M. Flower, T.C. Lindley, Electron backscattering diffraction study of acicular ferrite, bainite, and martensite steel microstructures, Mater. Sci. Technol. **16**, 26–40 (2000).
20. N. Takayama, G. Miyamoto, T. Furuhara, Effects of transformation temperature on variant pairing of bainitic ferrite in low carbon steel, Acta Mater. **60**, 2387–2396 (2012).
21. G. Liang et al., Effect of cooling rate on microstructure and mechanical properties of a low-carbon low-alloy steel, J. Mater. Sci. **56**, 3995–4005 (2021)
22. T. Kaneshita, G. Miyamoto, T. Furuhara, Variant selection in grain boundary nucleation of bainite in Fe-2Mn-C alloys, Acta Mater. **127**, 368–378 (2017)
23. B. Su, H.P. Lin, J.C. Kuo, et al. EBSD investigation on microstructure transformation in low carbon steel during continuous cooling, Can. Metall. Q. **53**, 352–361 (2014)
24. M. Graf, M. Kuntz, H. Autenrieth et al., Investigation of size effects due to different cooling rates of as-quenched martensite microstructures in a low-alloy steel, Appl. Sci. **10**, 1–15 (2020)
25. C. Cayron, B. Artaud, L. Briottet, Reconstruction of parent grains from EBSD data, Mater. Character. **57**, 386–401 (2006)
26. J.K. Mackenzie, The distribution of rotation axes in a random aggregate of cubic crystals, Acta Metall. **12**, 223–225 (1964)
27. G. Kurdjumov, G. Sachs, Über den Mechanismus der Stahlhärtung, Zeitschrift für Physik. **64**, 325–343 (1930)
28. Z. Nishiyama, X-ray investigation of the mechanism of the transformation from face centered cubic lattice to body centered cubic, Sci. Rep. Tohoku Univ. **23**, 637 (1934)
29. A.B. Greninger, A.Z. Troiano, The mechanism of martensite formation, Metals Trans. **185**, 590–598 (1949)
30. Y. Ohmori, H. Ohtsubo, Y.C. Jung et al., Morphology of Bainite and Widmanstätten Ferrite, Metall. Mater. Trans. A **25A**, 1981–1989 (1994)
31. D. Phelan, N. Stanford, R. Dippenaar, In situ observations of Widmanstätten ferrite formation in a low-carbon steel, Mater. Sci. Eng. A **407**, 127–134 (2005)
32. K.J. Irvine, F.B. Pickering, The tempering characteristics of low-carbon low-alloy steels, J. Iron Steel Inst. **194**, 137–153 (1960)
33. J.-B. Delattre, Private communication
34. J. K. Mackenzie, Second paper on statistics associated with the random disorientation of cubes, Biometrika, **44**, 229–240 (1957)
35. J.D. Watson, P.G. Mcdougallt, The crystallography of Widmanstätten ferrite, Acta Metall. **21**, 961–973 (1973)
36. S. Morito, H. Tanaka, R. Konishi et al., The morphology and crystallography of lath martensite in Fe-C alloys, Acta Mater. **51**, 1789–1799 (2003)
37. E. Bouyne, H.M. Flower, T.C. Lindley et al. Use of EBSD technique to examine microstructure and cracking in a bainitic steel, Scr. Mater. **39**, 295–300 (1998)

38. T. Zhou, H. Yu, S. Wang, Effect of microstructural types on toughness and microstructural optimization of ultra-heavy steel plate: EBSD analysis and microscopic fracture mechanism, Mater. Sci. Eng. A **658**, 150–158 (2016)
39. A.F. Gourgues, H.M. Flower, T.C. Lindley, Electron backscattering diffraction study of acicular ferrite, bainite, and martensite steel microstructures, Mater. Sci. Technol. **16**, 26–40 (2000)

Cite this article as: Anna Benarosch, B. Marini, C. Toffolon-Masclet, Z. Trzaska, E. Meslin, I. Guillot, Effect of cooling rate on the microstructures of three low carbon alloys with different manganese and molybdenum contents, Metall. Res. Technol. **119**, 520 (2022)